Nonhysteretic Superelasticity of Shape Memory Alloys at the Nanoscale

Zhen Zhang,[1,*] Xiangdong Ding,[1,†] Jun Sun,[1] Tetsuro Suzuki,[2] Turab Lookman,[3] Kazuhiro Otsuka,[2] and Xiaobing Ren[1,2,‡]

[1]*Multi-Disciplinary Materials Research Center, Frontier Institute of Science and Technology, and State Key Laboratory for Mechanical Behavior of Materials, Xi'an Jiaotong University, Xi'an 710049, China*

[2]*Ferroic Physics Group, National Institute for Materials Science, Tsukuba 305-0047, Ibaraki, Japan*

[3]*Theoretical Division, Los Alamos National Laboratory, Los Alamos, New Mexico 87545, USA*

(Received 11 April 2013; revised manuscript received 16 July 2013; published 30 September 2013)

We perform molecular dynamics simulations to show that shape memory alloy nanoparticles below the critical size not only demonstrate superelasticity but also exhibit features such as absence of hysteresis, continuous nonlinear elastic distortion, and high blocking force. Atomic level investigations show that this nonhysteretic superelasticity results from a continuous transformation from the parent phase to martensite under external stress. This aspect of shape memory alloys is attributed to a surface effect; i.e., the surface locally retards the formation of martensite and then induces a critical-end-point-like behavior when the system is below the critical size. Our work potentially broadens the application of shape memory alloys to the nanoscale. It also suggests a method to achieve nonhysteretic superelasticity in conventional bulk shape memory alloys.

DOI: 10.1103/PhysRevLett.111.145701 PACS numbers: 64.70.kd, 62.20.fg, 64.70.Nd, 81.30.Kf

Superelasticity, which refers to the ability of achieving much larger recoverable strains ($\sim 8\%$) than conventional metals and alloys [1,2], is known to appear in shape memory alloys (SMAs) possessing a spontaneous thermoelastic martensitic transformation [3]. Close to the transformation temperature, the high-symmetry parent phase can be deformed into low-symmetry martensite by external stress. Upon unloading, the martensite reversely transforms back to the parent phase. This stress-induced transformation corresponds to a macroscopic superelasticity [4]. For most SMAs, the generation and motion of internal interfaces (i.e., phase boundaries and twin boundaries) during the transformation dissipate a significant fraction of the total mechanical energy, hence giving rise to a hysteresis between the loading and unloading processes [5,6]. Superelasticity makes SMAs important functional materials not only in the macroscale but also in the micrometer scale [4,7,8].

Compared with their bulk counterpart, the potential applications of superelasticity of nanosized SMAs hinge on whether stress-induced transformation can persist down to several nanometers. Theoretical work indicates that phase transformations (e.g., ferroelectric transition and ferromagnetic transition) are less possible to occur in miniaturized systems [9,10]. Recent studies on nanosized SMAs (e.g., Ti-Ni, Fe-Pd, and Au-Cd) demonstrate that the martensitic transformation temperature lowers with reducing sample size, and the transformation vanishes below a critical size (usually several nanometers) [11–13]. As superelasticity of SMAs is closely related with the existence of a martensitic transformation, it is an intriguing question as to whether or not such a property can still exist below the critical size. Although experimental studies have shown the existence of superelasticity in SMAs at a size of 30 nm–150 μm [8,14,15] which is above the critical size, there exists no information about the superelasticity below the critical size. This is because of the great challenge in doing such an experiment.

In this Letter, by using molecular dynamics simulations, we provide atomic-level evidence on the existence of superelastic behavior of SMAs below their critical size. Being different from most bulk SMAs, this superelasticity is free of hysteresis and results from a continuous lattice distortion between the parent phase and martensite. We will show that the nonhysteretic superelasticity of nanosized SMAs is attributed to a surface effect, a new paradigm different from the conventional bulk elastic energy [1].

We studied the response of SMA nanoparticles to applied stress with a model SMA, the EAM potential of which was proposed by Voter-Chen [16] and adjusted by Farkas *et al.* [17]. This EAM potential was designed to reproduce a reversible symmetry-lowering martensitic transformation with a large hysteresis in bulk materials [18]. Moreover, the simulated transformation is suppressed with reducing system size [19], thus reproducing the generic behavior of SMAs at the nanoscale. However, one should not expect that such a semiempirical potential can reproduce the detailed properties of a specific SMA.

Spherical nanoparticles of this model SMA with diameter $D = 1.5$–20 nm were formed into the $B2$ structure with 11 at.% substitutional defects (i.e., $A_{61}B_{39}$). We also studied particles with other doping contents. Results similar to the present Letter were observed. In this work, free surface boundary conditions were applied in three dimensions. We first measured the martensite start temperature (M_s) and the austenite finish temperature (A_f) of nanoparticles by ramping the temperature from 1 to 1200 K

with a Nose-Hoover thermostat [19]. The nanoparticle was subsequently annealed at 300 K (parent phase) for 200 ps before loading. As Fig. 2(a) shows, compressive stress along the $[001]_{B2}$ direction was applied by two parallel planar indenters. The indenter stiffness was set as 3 eV/Å^3 [20,21]. The loading and unloading processes were performed by a stepwise adjustment of the distance between two indenters with a strain rate of 10^{-5} ps^{-1} [21,22]. The distance decrement at each step was $10^{-4}D$, followed by a relaxation for 10 ps. The stress and strain behavior of the nanoparticle was calculated by averaging the data over the last 9 ps. All computer simulations were performed in canonical ensembles with the LAMMPS code [23].

The relationship between the martensitic transformation and the size of nanoparticles is shown in Fig. 1(a). The transformation temperatures (M_s and A_f) decrease with reducing the particle diameter, and the transformation temperature $T_0[=(M_s + A_f)/2]$ varies linearly with $1/D$, consistent with that of Fe nanowires [24] and Ti-Ni nanoparticles [25]. In addition, the critical size (D_c) in Fig. 1(a) is 3 nm *below* which the spontaneous transformation vanishes.

Figure 1(b) shows that the parent phase is cubic ($B2$) with $a_0 = 2.876$ Å at 300 K. The parent phase transforms to an orthorhombic martensite ($B19$) with $a = 4.34$ Å, $b = 2.65$ Å, and $c = 4.16$ Å [Fig. 1(c)]. We characterize this transformation with three principal distortions [1]:

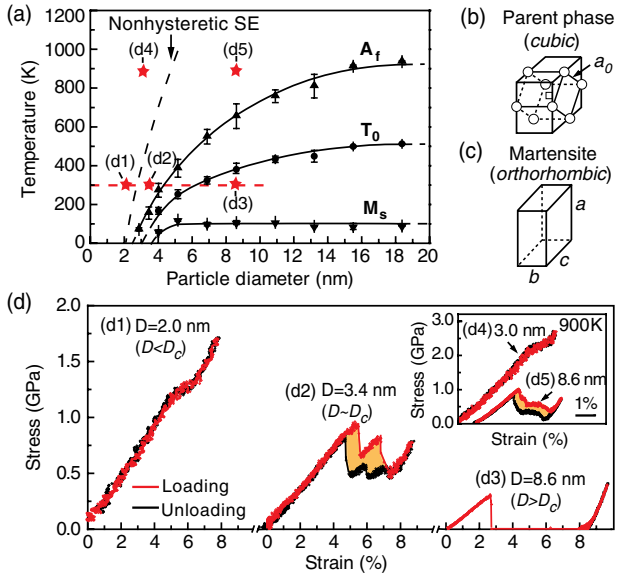

FIG. 1 (color online). (a) The relation between martensitic transformation and particle diameter (D). The dashed line indicates the border for nonhysteretic superelasticity obtained from Eq. (3). (b) and (c) The lattice correspondence between the parent phase and martensite. (d) Stress-strain curves of particles at 300 K with (d1) $D = 2.0$ nm, (d2) $D = 3.4$ nm, and (d3) $D = 8.6$ nm. Inset shows the stress-strain curves of particles at 900 K with (d4) $D = 3.0$ nm and (d5) $D = 8.6$ nm.

$\eta_1 = a/\sqrt{2}a_0 = 1.067$, $\eta_2 = b/a_0 = 0.92$, $\eta_3 = c/\sqrt{2}a_0 = 1.02$. The value of principal distortions of the model SMA is similar to that of Cu-14.2Al-4.3Ni (wt.%) alloy (i.e., 1.062, 0.917, and 1.023 [26]). Moreover, the present results could be applied to other SMAs, since the $B2$-$B19$ transformation is also observed in Au-Cd alloys, Ti-Ni-based alloys, and Ti-Pd-based high temperature alloys [1,27,28].

Stress-strain curves of nanoparticles at 300 K were studied in three typical size regimes $D < D_c$, $D \sim D_c$, and $D > D_c$. The stress-strain curve of the particle with $D = 8.6$ nm ($D > D_c$) is shown in Fig. 1(d3). The particle deforms elastically below 0.3 GPa, after which the stress decreases sharply to zero followed by an inelastic strain. Upon unloading, the particle cannot recover to its original shape, leading to 8% residual strain. The consistency of residual strain and transformation strain ($1 - \eta_2 = 0.08$) indicates a stress-induced martensitic transformation has occurred.

The stress-strain curve of the particle with $D = 3.4$ nm ($D \sim D_c$) is shown in Fig. 1(d2). This particle shows elastic deformation below 0.9 GPa, followed by a stress drop after which several discontinuous plateaus appear

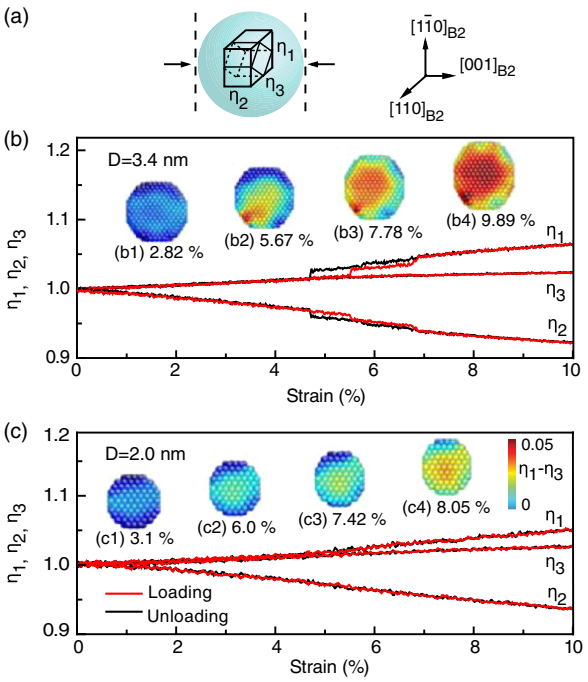

FIG. 2 (color online). (a) The relation between principal distortions (η_1, η_2, and η_3) and loading direction. (b) Principal distortions as a function of compressive strain for the particle with $D = 3.4$ nm. (b1)-(b4) Corresponding microstructures at strain of 2.82%, 5.67%, 7.78%, and 9.89% upon loading. (c) Principal distortions as a function of compressive strain for the particle with $D = 2.0$ nm. (c1)-(c4) Corresponding microstructures at strain of 3.1%, 6.0%, 7.42%, and 8.05% upon loading. Atoms are colored by $\eta_1 - \eta_3$, where $\eta_1 - \eta_3 = 0$ represents elastic distortion; $\eta_1 - \eta_3 > 0$ represents inelastic distortion to the orthorhombic phase.

with 2.5% inelastic strain. Upon unloading, the inelastic strain is fully recovered, demonstrating a superelastic behavior. It indicates that the parent phase is gradually stabilized by reducing the particle size. Moreover, the stress-strain curve of this particle shows hysteresis associated with the superelasticity between loading and unloading curves.

One of our interesting results is the stress-strain curve of the particle with $D = 2.0$ nm ($D < D_c$), for which the spontaneous martensitic transformation vanishes completely. As Fig. 1(d1) shows, this particle exhibits elastic deformation below 1.2 GPa; the stress then increases smoothly to 1.4 GPa with 1.5% inelastic strain. Upon unloading, the inelastic strain is fully recovered, and the hysteresis between loading and unloading curves disappears. Thus, the nanoparticle within our model SMA exhibits superelasticity below the critical size when compressed along the $[001]_{B2}$ direction. Moreover, this superelasticity is characterized by several interesting features such as the vanishing of hysteresis, continuous inelastic distortion, and high blocking force [29].

There are experimental findings consistent with the present simulation results. The nanograined Ti-Ni alloys made by severe plastic deformation show small hysteresis in their superelasticity contrasting with their bulk counterpart [14]. The thermal analysis indicates that the martensitic transformation of such nanograins becomes smeared. We expect that the size of nanograins may approach their critical size, and it is possible that the narrow-hysteretic superelasticity of nanograined Ti-Ni alloys is ascribed to the same origin as revealed by present results.

We now elaborate further on the average principal distortions η_1, η_2, and η_3 during the loading and unloading processes. As Fig. 2(b) shows, the particle with $D = 3.4$ nm deforms elastically at first, characterized by the same value of η_1 and η_3. Figure 2(b1) shows that no martensite appears in this regime. The elastic distortion of this particle is terminated by a steep splitting of η_1 and η_3, after which a martensite nucleus appears near the surface [Fig. 2(b2), red]. With further loading, the splitting between η_1 and η_3 keeps on increasing, corresponding to the growth of the martensite [Figs. 2(b3) and 2(b4)]. Upon unloading, η_1, η_2, and η_3 recover with a clear hysteresis in the transformation regime. Figure 2(b) demonstrates that the hysteretic superelasticity of the particle with $D = 3.4$ nm [Fig. 1(d2)] results from a stress-induced first-order martensitic transformation.

When $D = 2.0$ nm ($D < D_c$), the evolution of the average principal distortions and microstructure of nanoparticles exhibits quite different features [Fig. 2(c)]. This particle deforms elastically at first without the formation of martensite [Fig. 2(c1)]. Then, a splitting of η_1 and η_3 appears continuously, in contrast to the steep jump of principal distortions in larger particles [Fig. 2(b)]. Figures 2(c2)-2(c4) further confirm that the cubic parent phase is deformed continuously into the orthorhombic phase without sudden nucleation. The overlapping of loading and unloading curves for η_1, η_2, and η_3 demonstrates that this process is nonhysteretic. Thus, these direct microscopic results indicate that the nonhysteretic superelasticity observed in the particle with $D = 2.0$ nm [Fig. 1(d1)] results from a continuous lattice distortion between the cubic parent phase and the orthorhombic phase.

In the following, we explain phenomenologically the nonhysteretic superelasticity of SMAs at the nanoscale. SMA nanoparticles are different from bulk materials in that a large fraction of atoms are located at the surface. Since the surface breaks the translational invariance of the system, a different behavior on the stress-induced formation of martensite is expected near the surface as compared with the bulk. Thus, we investigated the spatial distribution of orthorhombic lattice distortions in particles during loading. As shown in Fig. 3, the orthorhombic lattice distortion is nonuniform in both particles with $D = 2.0$ and 3.4 nm, and a reduction of $\eta_1 - \eta_3$ appears near the free surface within almost two unit cells.

This core-shell picture enables us to divide the nanoparticle into interior and surface regions with a distinct free energy landscape [Fig. 4(a)]. The Landau-type free energy of the interior region is the same as that of bulk materials [30,31]. At the loading temperature ($M_s < T < T_0$), the free energy curve has three energy minima, with order parameter (orthorhombic lattice distortion) $e = 0$ representing the parent phase and the two minima with $|e| > 0$ representing the martensite. A large energy barrier between the parent phase and martensite exists and keeps the system in the parent phase prior to loading. Figure 4(a) further shows that the free energy of the surface region, being different from that of the interior, depends harmonically on e, resulting in only one energy minima at $e = 0$.

As the fraction of surface atoms changes, the free energy landscapes of particles with $D < D_c$, $D \sim D_c$, and $D > D_c$ are depicted as Figs. 4(b1), 4(b2), and 4(b3). The free energy of the particle with $D > D_c$ is similar to that of bulk. Its stress-strain curve [Fig. 4(d3)], obtained from the

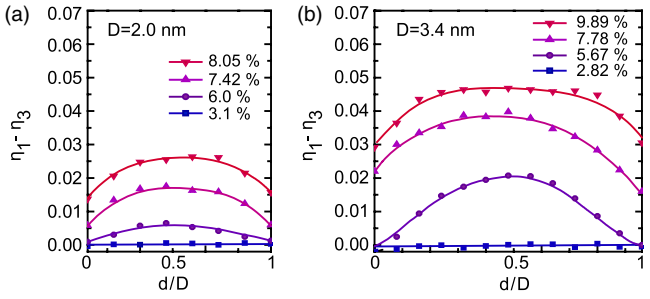

FIG. 3 (color online). Spatial distribution of orthorhombic lattice distortion $\eta_1 - \eta_3$ upon loading in particles with (a) $D = 2.0$ nm and (b) $D = 3.4$ nm.

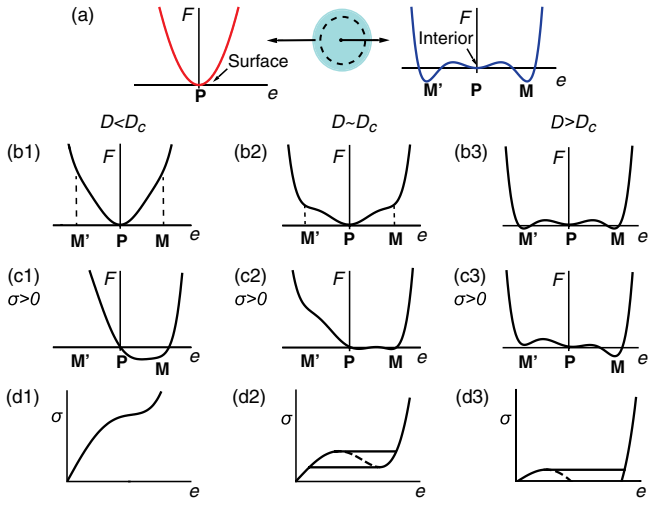

FIG. 4 (color online). (a) Free energy landscape of nanosized SMAs with interior and surface regions. P represents the parent phase; M and M' represent martensite. (b1), (b2), and (b3) Free energy curves of particles at 300 K with $D < D_c$, $D \sim D_c$, and $D > D_c$. (c1), (c2), and (c3) Corresponding tilted free energy curves upon loading. (d1), (d2), and (d3) Corresponding stress-strain curves obtained by taking variation of their free energy curves with respect to the order parameter e [30].

free energy curve [Fig. 4(b3)] [30], exhibits an irreversible inelastic strain upon loading, capturing the behaviors of the particle with $D = 8.6$ nm [Fig. 1(d3)]. For the particle with $D \sim D_c$, its free energy curve [Fig. 4(b2)] contains spinodals, giving rise to the presence of martensite with energy higher than the parent phase. With applied stress [Fig. 4(c2)], an energy barrier exists between the parent phase and the stress-induced martensite. As a result, the transformation occurs with the nucleation and growth of the martensite [32]. Its stress-strain curve [Fig. 4(d2)] shows superelasticity with hysteresis, reproducing the behavior of the particle with $D = 3.4$ nm [Fig. 1(d2)]. Below the critical size, the free energy curve of the particle has the form of Fig. 4(b1). With applied stress [Fig. 4(c1)], the energy barrier between the parent phase and martensite vanishes. Therefore, the transformation occurs without sudden nucleation of martensite and its stress-strain curve [Fig. 4(d1)] shows continuous inelastic distortion at a very high stress value without hysteresis, leading to the unusual behavior of the particle with $D = 2.0$ nm [Fig. 1(d1)].

As Figs. 4(b1), 4(c1), and 4(d1) show, the nonhysteretic superelasticity of SMAs at the nanoscale induced by surface is similar to the behaviors of bulk materials close to their critical endpoint induced by raising the temperature [30,33]. To achieve this state, the temperature of bulk SMAs should be increased to T_c^{SE} as

$$T_c^{\mathrm{SE}} = T_0 + 21B^2/80A_0C, \tag{1}$$

where T_0 is the transformation temperature and $A_0(>0)$, $B(<0)$, $C(>0)$ are coefficients of the 2-4-6 type Landau potential for martensitic transformation [30]. At the nanoscale, the transformation temperature T_0 correlates with system size D as

$$T_0 = T_0^B - (2g/A_0\delta)D^{-1}, \tag{2}$$

where T_0^B is the transformation temperature in bulk, g is the coefficient of the gradient energy, and δ is a phenomenological parameter characterizing the surface effect [19]. Then, the critical size D_c^{SE} below which the hysteresis of superelasticity vanishes can be deduced from Eqs. (1) and (2) as

$$D_c^{\mathrm{SE}} = (2g/A_0\delta)(T_0^B + 21B^2/80A_0C - T)^{-1}. \tag{3}$$

D_c^{SE} of the present model SMA can be calculated by Eq. (3). In this work, the parameters of Eq. (3) are obtained from the curves of Fig. 1(a). The fitting between T_0 and D with Eq. (2) gives rise to $T_0^B \sim 596$ K and $2g/A_0\delta \sim 1773$ K $\cdot$ nm. The value of B^2/A_0C is obtained approximately from the temperature difference between A_f and T_0 as $\sim 16(A_f - T_0)$ [30]. Then, the calculated D_c^{SE} is depicted in Fig. 1(a).

We compare the simulation results with the analytical ones at 300 K and elevated temperature. At 300 K, the calculated D_c^{SE} is ~ 2.8 nm, consistent with simulated results that the particle exhibits nonhysteretic superelasticity when $D = 2.0$ nm. At 900 K, the calculated D_c^{SE} is ~ 5.2 nm. Consistently, we observe the nonhysteretic superelasticity for the particle with $D = 3.0$ nm [Fig. 1(d4)], while large hysteresis appears for the particle with $D = 8.6$ nm [Fig. 1(d5)]. The sharp increase of D_c^{SE} with increasing size [Fig. 1(a)] further shows that to obtain nonhysteretic superelasticity at even larger size requires a much higher loading temperature beyond the melting point (~ 1500 K here), hence becomes infeasible.

Note that the present model SMA exhibits nonhysteretic behavior below its critical size, even though it possesses hysteretic superelasticity at larger scale [Fig. 1(d)]. Our simulations thus have indicated that nonhysteretic superelasticity can be achieved with conventional SMAs (especially with large hysteresis) by merely reducing their size (e.g., nanoparticles or nanograins). Previous studies on nanograined Ti-Ni alloys seem to support this possibility [14]. Therefore, the mechanical properties of other SMAs at the nanoscale would be interesting to study experimentally. In addition, since other ferroic transitions also show a similar size effect (e.g., ferroelectric transition [34]), a giant nonhysteretic response similar to this work may be found at the nanoscale.

Since the nanoparticles are free-standing in the present work, the constraint imposed by neighboring grains within a bulk material is not taken into account. A more general framework would have to include the effect of boundary conditions (i.e., free-standing or grains in a bulk material)

on transformation. Further studies are needed to address this interesting issue.

In summary, we have shown that SMAs can exhibit nonhysteretic superelasticity at the nanoscale. This behavior results from a surface-dominated continuous transformation from the parent phase to martensite. Our results have potential applications to the study of nanosized SMAs in energy storage and conversion devices and sensors where large nonhysteretic strain is expected. Moreover, our work provides a simple guideline to design new functional materials with a giant nonhysteretic response to the external field.

The authors gratefully acknowledge the support of the National Basic Research Program of China (Grants No. 2012CB619401 and No. 2010CB613003), National Natural Science Foundation of China (Grants No. 51171140, No. 51231008, No. 51320105014, No. 51321003, and No. 51222104), as well as 111 project of China (Grant No. B06025). X. R. acknowledges the financial support from Kakenhi.

*Corresponding author.
zhenn.zhang@gmail.com
†dingxd@mail.xjtu.edu.cn
‡REN.Xiaobing@nims.go.jp

[1] K. Otsuka and C. M. Wayman, *Shape Memory Materials* (Cambridge University Press, Cambridge, England, 1998).
[2] Y. Tanaka, Y. Himuro, R. Kainuma, Y. Sutou, T. Omori, and K. Ishida, Science **327**, 1488 (2010).
[3] A. G. Khachaturyan, *Theory of Structural Transformation in Solid* (Wiley & Sons, New York, 1983).
[4] K. Otsuka and T. Kakeshita, MRS Bull. **27**, 9 (2002).
[5] R. B. Pérez-Sáez, V. Recarte, M. L. Nó, and J. S. Juan, Phys. Rev. B **57**, 5684 (1998).
[6] J. Van Humbeeck, J. Alloys Compd. **355**, 58 (2003).
[7] T. W. Duerig, MRS Bull. **27**, 101 (2002).
[8] J. S. Juan, M. L. Nó, and C. A. Schuh, Nat. Nanotechnol. **4**, 415 (2009).
[9] M. Kaganov and A. Omel'Yanchuk, Sov. Phys. JETP **34**, 895 (1972).
[10] A. M. Bratkovsky and A. P. Levanyuk, Phys. Rev. Lett. **94**, 107601 (2005).
[11] T. Waitz, V. Kazykhanov, and H. Karnthaler, Acta Mater. **52**, 137 (2004).
[12] K. Seki, H. Kura, T. Sato, and T. Taniyama, J. Appl. Phys. **103**, 063910 (2008).
[13] K. Asaka, Y. Hirotsu, and T. Tadaki, Mater. Sci. Eng. A **312**, 232 (2001).
[14] K. Tsuchiya, M. Inuzuka, D. Tomus, A. Hosokawa, H. Nakayama, K. Morii, Y. Todaka, and M. Umemoto, Mater. Sci. Eng. A **438–440**, 643 (2006).
[15] S. M. Ueland, Y. Chen, and C. A. Schuh, Adv. Funct. Mater. **22**, 2094 (2012).
[16] A. F. Voter and S. P. Chen, Mater. Res. Soc. Symp. Proc. **82**, 175 (1986).
[17] D. Farkas, B. Mutasa, C. Vailhe, and K. Ternes, Model. Simul. Mater. Sci. Eng. **3**, 201 (1995).
[18] N. P. Lazarev, C. Abromeit, R. Schaublin, and R. Gotthardt, J. Appl. Phys. **100**, 063520 (2006).
[19] Z. Zhang, X. Ding, J. Deng, J. Cui, J. Sun, T. Suzuki, K. Otsuka, and X. Ren, J. Phys. Chem. C **117**, 7895 (2013).
[20] C. L. Kelchner, S. J. Plimpton, and J. C. Hamilton, Phys. Rev. B **58**, 11 085 (1998).
[21] G. Ziegenhain and H. M. Urbassek, Phys. Rev. B **81**, 155456 (2010).
[22] H. S. Park, K. Gall, and J. A. Zimmerman, Phys. Rev. Lett. **95**, 255504 (2005).
[23] S. J. Plimpton, J. Comput. Phys. **117**, 1 (1995).
[24] L. Sandoval and H. M. Urbassek, Nano Lett. **9**, 2290 (2009).
[25] D. Mutter and P. Nielaba, Eur. Phys. J. B **84**, 109 (2011).
[26] K. Otsuka and K. Shimizu, Trans. Jpn. Inst. Metals **15**, 103 (1974).
[27] D. S. Lieberman, M. S. Wechsler, and T. A. Read, J. Appl. Phys. **26**, 473 (1955).
[28] Y. Y. Ye, C. T. Chan, and K. M. Ho, Phys. Rev. B **56**, 3678 (1997).
[29] W.-F. Rao, M. Wuttig, and A. G. Khachaturyan, Phys. Rev. Lett. **106**, 105703 (2011).
[30] F. Falk, J. Phys. Colloq. **43**, C4-3 (1982).
[31] E. K. H. Salje, *Phase Transitions in Ferroelastic and Co-elastic Crystals* (Cambridge University Press, Cambridge, England, 1990).
[32] J. W. Christian, *The Theory of Transformations in Metals and Alloys* (Pergamon Press, Oxford, 2002).
[33] P. Limelette, A. Georges, D. Jérome, P. Wzietek, P. Metcalf, and J. M. Honig, Science **302**, 89 (2003).
[34] D. D. Fong, G. B. Stephenson, S. K. Streiffer, J. A. Eastman, O. Auciello, P. H. Fuoss, and C. Thompson, Science **304**, 1650 (2004).